Pulsed-gate measurements of the singlet-triplet relaxation time in a two-electron double quantum dot

J. R. Petta,[1] A. C. Johnson,[1] A. Yacoby,[1,2] C. M. Marcus,[1] M. P. Hanson,[3] and A. C. Gossard[3]

[1]*Department of Physics, Harvard University, Cambridge, Massachusetts 02138, USA*
[2]*Department of Condensed Matter Physics, Weizmann Institute of Science, Rehovot 76100, Israel*
[3]*Materials Department, University of California, Santa Barbara, California 93106, USA*

A pulsed-gate technique with charge sensing is used to measure the singlet-triplet relaxation time for nearly degenerate spin states in a two-electron double quantum dot. Transitions from the (1,1) charge occupancy state to the (0,2) state, measured as a function of pulse cycle duration and magnetic field, allow the (1,1) singlet-triplet relaxation time ($\geqslant 70$ μs) and the (0,2) singlet-triplet splitting to be measured. This technique can be readily applied to read out a spin-qubit operating in a singlet-triplet basis.

Semiconductor quantum dots are promising systems for the manipulation of electron spin because of the relative ease of confining and measuring single electrons.[1] A spin memory based on electron-spin orientation requires a long spin-relaxation time, T_1. For coherent manipulation of electronic-spin states, the spin dephasing time T_2 is the important figure of merit because it sets the time scale in which coherent operations must be performed. In order to make use of the spin degree of freedom as a holder of either classical or quantum information, it is first necessary to understand and characterize the mechanisms that lead to spin relaxation and decoherence.

Previous studies of spin relaxation in quantum dots have focused on systems with large spin splittings. Relaxation times for spin states separated by a singlet-triplet splitting $E_{ST} \sim 600$ μeV have been shown[2] to approach 200 μs. Several groups have measured spin relaxation for Zeeman split spin states at high fields ($E_{Zeeman} \sim 200$ μeV), demonstrating long T_1 times.[3–5] Since the readout techniques used in these experiments require coupling to the leads, the spin splitting must be larger than the thermal energy for accurate spin-state readout. At dilution refrigerator temperatures, this implies that $E_{Zeeman} > k_B T \sim 10$ μeV, or $B > 0.5$ T. For $B > 0.5$ T, T_1 shows a strong field dependence, as is expected theoretically for spin-orbit-mediated spin-relaxation processes.[6,7]

Hyperfine interactions, coupled with phonon emission, can also lead to spin relaxation. The hyperfine interaction results in an effective magnetic field, $B_{nuc} \sim 4$ T$/\sqrt{N_E} \sim 2$ mT, where $N_E \sim 5 \times 10^6$ is the effective number of nuclei interacting with the electron spin for typical GaAs quantum dots.[8–10] When the splitting between spin states is on the order of, or less than, the hyperfine energy scale, the hyperfine interaction can result in electron-spin relaxation. Since $B_{nuc} \sim 2$ mT ~ 0.05 μeV $\ll k_B T$, a spin readout that can distinguish between nearly degenerate spin states is required to measure T_1 in this regime.

In this paper we describe an experimental technique that allows measurements of the singlet-triplet relaxation time for nearly degenerate two-electron spin states. This technique can be used to measure T_1 in regimes for which hyperfine-mediated relaxation processes are expected to be important. Spin relaxation between nearly degenerate electronic states is particularly relevant to the problem of controlled entanglement, as the singlet-triplet splitting goes to zero as the entangled spins become spatially separated. We also note that the technique presented in this paper can be easily extended to read out a spin qubit based on singlet-triplet states.[11]

Measurements are performed using a few-electron double quantum dot fabricated from a GaAs/Al$_{0.3}$Ga$_{0.7}$As heterostructure grown by molecular-beam epitaxy. Electron-beam lithography and liftoff are used to create Ti/Au gates that deplete a 100-nm-deep two-dimensional electron gas with electron density 2×10^{11} cm^{-2} and mobility 2×10^5 cm^2/V s. Gates 2–6 and 12 form the double quantum dot [see Fig. 1(a)]. Gates 2 and 6 are connected via bias tees to dc voltage sources and to pulse generators through coaxial cables with ~ 20 dB of inline attenuation.[12] A quantum point contact (QPC) charge detector is created by depleting gate 1. Gates 7–11 are unused. The QPC conductance, G_S, is measured using standard lock-in amplifier techniques with a 1-nA current bias at 93 Hz. The electron temperature, $T_e \sim 135$ mK, was determined from Coulomb blockade peak widths. We present results from a single sample; a second sample with slightly larger lithographic dimensions gave qualitatively similar results.[13]

QPC charge sensing is used to determine the absolute number of electrons in the double dot. Figure 1(b) shows a large-scale charge stability diagram for the double dot. As electrons enter or leave the double dot, or transfer from one dot to the other, G_S changes, resulting in sharp features in dG_S/dV_6 (numerically differentiated).[13,14] In the lower left corner of Fig. 1(b), the double dot is completely empty. As the gate voltages are made more positive, electrons are added to the double dot. We will focus on the two-electron regime near the (1,1) to (0,2) charge transition (integer pairs specify the equilibrium charge occupancy on the left and right dot) [Fig. 1(c)].

In the two-electron regime, charge transport in a double dot shows a striking asymmetry in bias voltage due to spin-selection rules (Pauli blocking).[15,16] This asymmetry is due to the different singlet-triplet splittings in the (1,1) and (0,2)
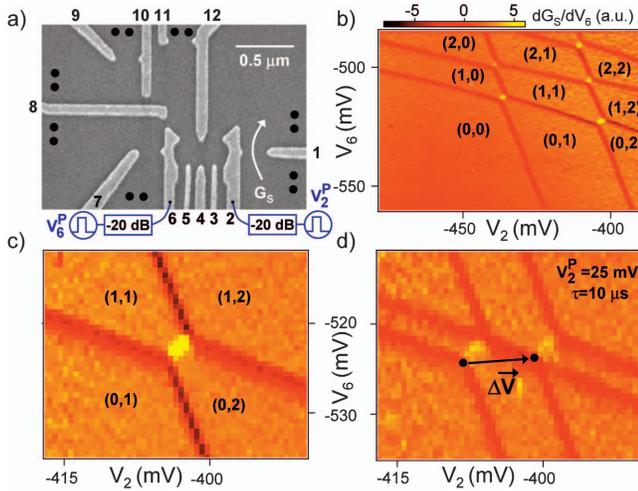
FIG. 1. (Color) (a) Scanning electron microscopy (SEM) image of a device identical in design to the one used in this experiment. Gates 2–6 and 12 define the double dot. (●) denotes an ohmic contact. (b) Large-scale plot of dG_S/dV_6 as a function of V_2 and V_6. Charge states are labeled (M,N), where $M(N)$ is the time-averaged number of electrons on the left (right) dot. (c) Zoom in near the $(1,1)$ to $(0,2)$ charge transition. (d) 25 mV pulses with a 50% duty cycle and 10-μs period are applied to the coax connected to gate 2. This results in two copies of the charge stability diagram shifted relative to one another by $\vec{\Delta V}$.

charge states. Spin states of the weakly coupled $(1,1)$ charge configuration are nearly degenerate, while the $(0,2)$ spin states are separated by a ~ 400 μeV singlet-triplet splitting, J. At forward bias, transitions from the $(0,2)$ singlet state, $(0,2)_S$, to the $(1,1)$ singlet state, $(1,1)_S$, are allowed. However, for reverse bias, $(1,1)$ to $(0,2)$ transitions can be blocked if the $(1,1)$ state forms a triplet $(1,1)_T$ because the $(0,2)_T$ state resides outside the transport window due to the large singlet-triplet splitting in $(0,2)$. This asymmetry results in current rectification, which will be used in the present pulsed-gate experiment for spin to charge conversion.

Charge transitions are driven by applying pulses to gates 2 and 6. Pulse heights are calibrated by applying pulses to a single gate and measuring the charge stability diagram. Figure 1(d) shows a charge stability diagram acquired with square pulses applied to gate 2 ($V_2^P = 25$ mV, 50% duty cycle, period $\tau = 10$ μs). This results in two copies of the charge stability diagram; the right-most (left-most) charge stability diagram reflects the ground-state charge configuration during the low (high) stage of the pulse sequence. The gate-voltage offset between the charge stability diagrams, $\vec{\Delta V}$, is used to calibrate pulse amplitudes. Due to attenuation in the coax cables, $\vec{\Delta V}$ is less than the pulse amplitude at the signal generator, V_2^P. Additional calibrations are performed for gate 6, which primarily shifts the honeycomb in the vertical direction (not shown). The charge stability diagram can be shifted in any direction in gate space by simultaneously applying calibrated pulses to gates 2 and 6.

In a double dot, charge can be pumped by pulsing gates around a triple point, e.g. $(0,1) \rightarrow (1,1) \rightarrow (0,2) \rightarrow (0,1)$. Our spin-relaxation measurement technique relies on the fact
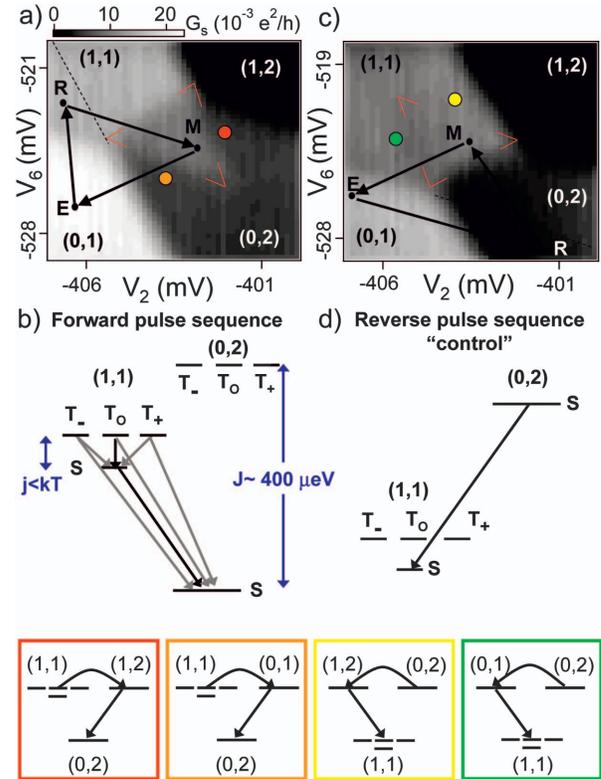

FIG. 2. (Color) (a) Sensor conductance, G_S, as a function of V_2 and V_6 while applying the forward pulse sequence (see text) with $\tau = 10$ μs and $B_\perp = 100$ mT. Spin-blocked transitions result in some $(1,1)$ charge signal in the $(0,2)$ pulse triangle (bounded by the red lines). Outside of the pulse triangle it is possible to access other charge states. This relaxes the spin blockade (see color-coded level diagrams). (b) Level diagram illustrating the possible transitions from $(1,1)$ to $(0,2)$. The black arrows indicate fast transitions; the gray arrows indicate spin-blocked transitions. (c) G_S as a function of V_2 and V_6 while applying the reverse "control" pulse sequence with $\tau = 10$ μs and $B_\perp = 100$ mT. The $(0,2)_S$ to $(1,1)_S$ transition is not spin blocked. As a result, there is no detectable pulse signal in the pulse triangle (bounded by the red lines). (d) Level diagram illustrating the $(0,2)$ to $(1,1)$ transition. A best-fit plane has been subtracted from the data in (a) and (c) to remove signal from direct gate to QPC coupling.

that $(1,1)_T$ to $(0,2)_S$ transitions are spin blocked. Measuring this charge transition probability as a function of time using charge sensing allows a T_1 measurement. Two control experiments, discussed below, demonstrate that the observed time dependence of the charge sensing signal is due to spin-blocked transitions.

T_1 is measured using a forward pulse sequence $(0,1) \rightarrow (1,1) \rightarrow (0,2) \rightarrow (0,1)$ as shown in [Fig. 2(a)]. The sequence begins with the gates at point E for 10% of the period, emptying the second electron from the double dot, leaving the $(0,1)$ charge state. The gates then shift to the reset point R for the next 10% of the period, which initializes the system into the $(1,1)$ configuration. The interdot tunnel coupling, t, is tuned with $t \lesssim k_B T$ so that the $(1,1)$ singlet-triplet splitting $j \sim 4t^2/U \ll k_B T$, where U is the single dot charging energy. Due to this degeneracy, and at low fields such that

$|g|\mu_B B < k_B T$ ($|g| \sim 0.44$ for GaAs), we expect to load into $(1,1)_S$ or any of the three $(1,1)_T$ states with equal probability. For the final 80% of the period, the gates are at the measurement point M where $(0,2)_S$ is the ground state. Figure 2(b) illustrates the possible $(1,1)$ to $(0,2)$ transitions. If the R step loads the $(1,1)_S$ state, tunneling to $(0,2)_S$ occurs on a time scale given by the interdot tunneling rate, $\Gamma(\epsilon)$ [we estimate the slowest $\Gamma(\epsilon)$ $(1~\mu s)^{-1}$ from finite bias data[16]]. If the $m_s = 0$ $(1,1)$ triplet state $(1,1)_{T0}$ is loaded, it dephases into $(1,1)_S$ on a time scale of T_2 (expected to be $\lesssim 100$ ns). (Refs. 10, 17, and 18) followed by a direct transition to $(0,2)_S$. About half the time the R step will load the $m_s = 1$ $(1,1)$ triplet state $(1,1)_{T+}$ or the $m_s = -1$ $(1,1)$ triplet state $(1,1)_{T-}$. At low $B_\perp$ $(0,2)_T$ is inaccessible, and a transition from $(1,1)_{T+}$ or $(1,1)_{T-}$ to $(0,2)$ requires a spin flip and will be blocked for times shorter than the singlet-triplet relaxation time τ_{ST}.

In Fig. 2(a) the average charge sensor signal, G_S, is measured as a function of the dc gate voltages V_2 and V_6, while a pulse sequence is repeated. This has the effect of translating the points E, R, and M throughout the charge stability diagram, keeping their relative positions constant. Because most of the time is spent at point M, the grayscale data primarily map out the ground-state population for this point, with plateaus at $G_S \sim 0.0$, 6.0, 16, and 23×10^{-3} e^2/h indicating full population of the (1,2), (0,2), (1,1), and (0,1) charge states, respectively. The pulse data differ from ground-state data only when point M resides in the triangle defined by the $(1,1)$ to $(0,2)$ ground-state transition and the extensions of the $(1,1)$ to $(0,1)$ and $(1,1)$ to $(1,2)$ ground-state transitions [bounded by the red marks in Fig. 2(a)]. Within this "pulse triangle" transitions from $(1,1)$ to $(0,2)$ may be blocked as described above, and the charge sensor registers a conductance intermediate between the $(1,1)$ and $(0,2)$ plateaus. If M moves above the pulse triangle [red dot in Fig. 2(a)], the $(1,1)$ to $(0,2)$ transition can occur sequentially via $(1,2)$ with no interdot tunneling: a new electron enters the right dot, then the electron in the left dot leaves. Likewise, if M moves below the pulse triangle [orange dot in Fig. 2(a)] the transition can occur via $(0,1)$: the left-dot electron leaves, then a new electron enters the right dot. By similar logic, point R must be to the left of the $(0,1)$ to $(0,2)$ transition extension [dotted line in Fig. 2(a)] to avoid resetting through $(0,2)$ and preferentially loading $(1,1)_S$. Figure 2(a) shows a signal of 11×10^{-3} e^2/h in the pulse triangle for $\tau = 10$ μs, which indicates that approximately 50% of the time the dots remain in $(1,1)$ even though $(0,2)$ is the ground state. This is direct evidence of spin-blocked $(1,1)$ to $(0,2)$ transitions.

As a control, we compare the forward T_1 pulse sequence with a reverse pulse sequence that does not involve spin-selective transitions $(0,1) \rightarrow (0,2) \rightarrow (1,1) \rightarrow (0,1)$. With the pulse sequence reversed the reset position R occurs in $(0,2)$ where only the singlet state is accessible, and M occurs in $(1,1)$. Now tunneling from R to M should always proceed on a time scale set by the interdot tunnel coupling, since the $(0,2)_S$ to $(1,1)_S$ transition is not spin blocked. As anticipated, no signal is seen in the pulse triangle for this reversed "control" sequence [Fig. 2(c)].

Spin selectivity of the forward pulse sequence in Fig. 3 can be used to measure J as a function of $B_\perp$ (Ref. 19). This
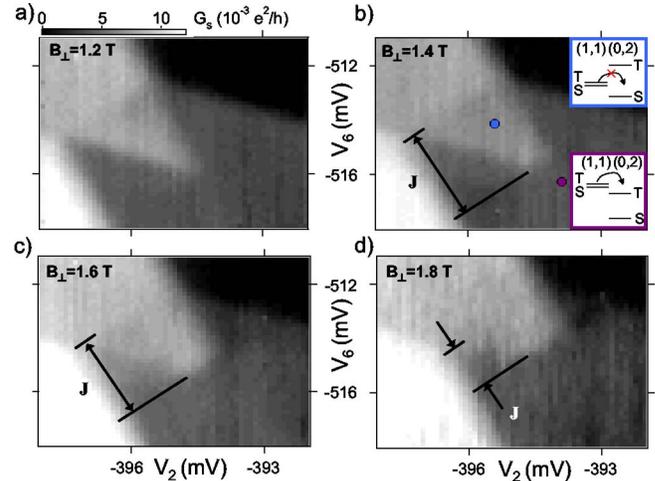

FIG. 3. (Color online) Forward pulse sequence results with $\tau = 10$ μs. (a)–(d) G_s as a function of V_2 and V_6 for increasing $B_\perp$. $B_\perp$ reduces J. Eventually $(0,2)_T$ is lowered into the "M" pulse window [inset of (b)]. At this point, $(1,1)_T$ to $(0,2)_T$ transitions are energetically possible and the transition from the $(1,1)$ to $(0,2)$ charge state is no longer "spin blocked." This cuts off the tip of the pulse triangle in $(0,2)$ [see (b)]. A best-fit plane has been subtracted from the data in (a)–(d).

also confirms that the charge sensing signal in the pulse triangle is due to spin-blocked interdot charge transitions. Figure 3(a) shows G_S as a function of V_2 and V_6 while applying the forward pulse sequence with $B_\perp = 1.2$ T and $\tau = 10$ μs. For these data, $(0,2)_T$ resides outside of the pulse triangle ($J > E_M$, the mutual charging energy) and the $(1,1)_T$ to $(0,2)$ transitions are spin blocked. For $B_\perp = 1.4$ T [Fig. 3(b)] the $(0,2)_T$ state is low enough in energy that the $(1,1)_T$ states can directly tunnel to the $(0,2)_T$ manifold at high detunings. Now $(1,1)$ to $(0,2)$ tunneling can proceed, and there is no longer a $(1,1)$ charge signal in the $(0,2)$ region of the pulse triangle at high detuning. This cuts off the tip of the pulse triangle. The spin-blocked region continues to shrink as $B_\perp$ is increased. From these data, we find $J \sim 340$, 280, and 180 μeV for $B_\perp = 1.4$, 1.6, and 1.8 T, respectively.[20]

The time dependence of the charge sensing signal can be investigated by varying τ, the overall period of the cycle. Figure 4(a) shows G_S as a function of V_2 and V_6 acquired using the forward pulse sequence with $\tau = 8$ μs at $B_\perp = 100$ mT. A clear pulse signal is observed in the pulse triangle. As τ is increased, the pulse signal decreases as shown in (b) and (c). G_S is measured inside the pulse triangle (V_2, V_6 held fixed at $-403, -523.8$ mV, respectively) and is plotted as a function of τ in Fig. 4(d). In $(1,1)$, $G_S \sim 20 \times 10^{-3}$ e^2/h, whereas outside the pulse triangle in $(0,2)$, $G_S \sim 10 \times 10^{-3}$ e^2/h. For small τ, $G_S \sim 15 \times 10^{-3}$ e^2/h in the pulse triangle. At long τ, G_S approaches 10×10^{-3} e^2/h in the pulse triangle, which indicates complete transfer from the $(1,1)$ to $(0,2)$ charge state.

These data are consistent with spin-blocked transitions preventing the $(1,1)$ to $(0,2)$ charge transition. Approximately 50% of the time, the $(1,1)$ R pulse loads into either $(1,1)_{T+}$ or $(1,1)_{T-}$. These states may relax into the $(1,1)_S$ state and then tunnel to $(0,2)_S$ on a time scale set by τ_{ST}. For $\tau \ll \tau_{ST}$, we
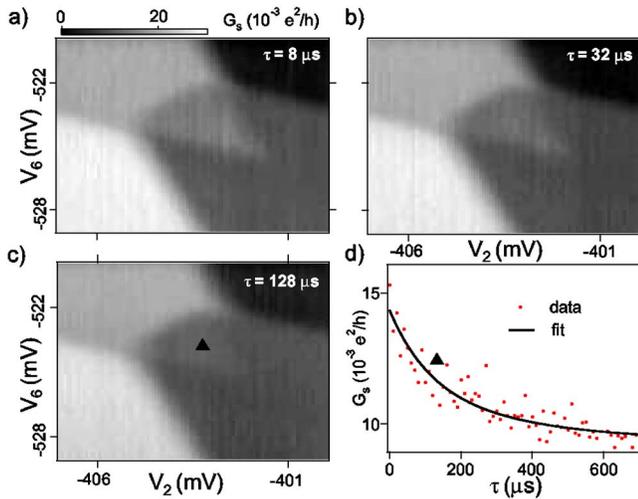
FIG. 4. (Color online) Forward pulse sequence results with $B_\perp = 100$ mT. (a)-(c) G_S as a function of V_2 and V_6 for increasing pulse periods, τ. For longer periods, singlet-triplet relaxation occurs and the (1,1) to (0,2) transition proceeds, reducing the signal in the (0,2) pulse triangle. (d) G_s with $V_2 = -403.0$ mV, $V_6 = -523.8$ mV [gate voltage position indicated by the black triangle in (c)] measured as a function of τ. $G_s = 10 \times 10^{-3}$ e^2/h in the (0,2) charge state, while $G_s = 20 \times 10^{-3}$ e^2/h in the (1,1) charge state. For short τ, the (1,1) to (0,2) transition is blocked approximately half of the time, resulting in a pulse signal of 15×10^{-3} e^2/h in the (0,2) pulse triangle. The (1,1) to (0,2) transition probability increases (sensor signal decreases) with τ due to spin relaxation with a characteristic time scale of 70 ± 10 μs. A best-fit plane has been subtracted from the data in (a)–(c).

expect that 50% of the (1,1) to (0,2) transitions will be spin blocked, resulting in $\sim$50% (1,1) pulse signal in the (0,2) pulse triangle. For $\tau > \tau_{ST}$, the $(1,1)_{T+}$ and $(1,1)_{T-}$ states have

ample time to relax to $(1,1)_S$, after which a $(1,1)_S$ to $(0,2)_S$ transition can take place. Thus, for τ long compared to τ_{ST}, the pulse signal approaches the (0,2) level, indicating full transfer of the (1,1) state to (0,2) state. In the intermediate τ regime, the sensor signal due to spin-blocked transitions decays as a function of time on a time scale that is characteristic of τ_{ST}.

The experimental data in Fig. 4(d) are fit assuming exponential singlet-triplet relaxation. Due to the slow measurement rate of the charge sensor ($\sim$100 ms), G_S is proportional to the time-averaged occupation of the left dot. Modeling an exponential decay of the sensing signal weighted over 80% of the cycle corresponding to the (0,2) measurement gives $G_S(\tau) = A + B(\tau_{ST}/\tau)(1 - e^{-0.8\tau/\tau_{ST}})$, where A is the conductance asymptote at long times [full occupation of the (0,2) state] and B is the additional conductance in a short pulse due to the blocked states [approximately 50% of the (0,2) to (1,1) step height]. The best fit to the data in Fig. 4(d) gives $A = 0.009$ e^2/h and $B = 0.007$ e^2/h, consistent with these expectations. In the center of the pulse triangle the best-fit τ_{ST} reaches a maximum of $\tau_{ST} = 70 \pm 10$ μs. Near the (1,1) to (0,2) transition, τ_{ST} decreases, to 20 ± 5 μs at $V_2 = -403.8$ mV and $V_6 = -523.0$ mV. Closer to the tip of the pulse triangle, τ_{ST} decreases due to thermally activated exchange with the leads (see Fig. 2, red and orange diagrams), thus the 70-μs relaxation time represents a lower bound on the spin-relaxation time within the (1,1) manifold.[21] This technique can be used to explore the full dependence of the spin-relaxation time on detuning and magnetic field.[22]

[1] M. Ciorga *et al.*, Phys. Rev. B **61**, R16315 (2000).
[2] T. Fujisawa *et al.*, Nature **419**, 278 (2002).
[3] R. Hanson *et al.*, Phys. Rev. Lett. **91**, 196802 (2003).
[4] J. M. Elzerman *et al.*, Nature **430**, 431 (2004).
[5] M. Kroutvar *et al.*, Nature **432**, 81 (2004).
[6] A. V. Khaetskii and Y. V. Nazarov, Phys. Rev. B **61**, 12639 (2000).
[7] V. N. Golovach, A. Khaetskii, and D. Loss, Phys. Rev. Lett. **93**, 016601 (2004).
[8] M. Dobers *et al.*, Phys. Rev. Lett. **61**, 1650 (1988).
[9] S. I. Erlingsson, Y. V. Nazarov, and V. I. Fal'ko, Phys. Rev. B **64**, 195306 (2001).
[10] A. V. Khaetskii, D. Loss, and L. Glazman, Phys. Rev. Lett. **88**, 186802 (2002).
[11] J. R. Petta *et al.*, Science **309**, 2180 (2005).
[12] We use Anritsu K251 bias tees. Tektronix AWG520 pulse generators are used for high speed manipulation of the gate voltages.

[13] J. R. Petta *et al.*, Phys. Rev. Lett. **93**, 186802 (2004).
[14] J. M. Elzerman *et al.*, Phys. Rev. B **67**, 161308(R) (2003).
[15] K. Ono *et al.*, Science **297**, 1313 (2002).
[16] A. C. Johnson *et al.*, Phys. Rev. B **72**, 165308 (2005).
[17] J. M. Kikkawa and D. D. Awschalom, Phys. Rev. Lett. **80**, 4313 (1998).
[18] I. A. Merkulov, Al. L. Efros, and M. Rosen, Phys. Rev. B **65**, 205309 (2002).
[19] R. C. Ashoori *et al.*, Phys. Rev. Lett. **71**, 613 (1993).
[20] The conversion from gate voltage to energy is determined by measuring finite bias triangles.
[21] $\Gamma(\epsilon)$ is set to be much faster than the characteristic relaxation times that we measure in this experiment. $\Gamma(\epsilon)$ varies strongly with ϵ (see Ref. 13). The fact that τ_{ST} only varies by roughly a factor of 3 in the pulse triangle also indicates that the (1,1)–(0,2) transitions are spin blocked and not limited by a slow $\Gamma(\epsilon)$.
[22] A. C. Johnson *et al.*, Nature (London) **435**, 925 (2005).